Design and Demonstration of a Passive Pitch System for Tidal Turbines

Stefano Gambuzza, Shūji Ōtomo, Yabin Liu, Anna M. Young, Riccardo Broglia, Mario Felli, Edward D. McCarthy, and Ignazio Maria Viola

Abstract—**Tidal turbines operate in unsteady and non-uniform flows, conditions that give rise to large fluctuations in the loads generated. Previous studies [1], [2] have shown that allowing for the blades of a tidal turbine to passively pitch around a longitudinal axis can reduce the fluctuations in thrust and torque due to shear and turbulence. In this work, we investigate the effects of steady changes in the inflow velocity and direction on the loads generated by a turbine equipped with passively pitching blades. We do so by presenting the results of an experimental campaign conducted in the large recirculating water channel at the Institute of Marine Engineering in Rome, in which the turbine was subject to flows with different freestream speeds and yaw angles. Results show that a turbine equipped with passively pitching blades produces more power than one with rigid blades when the freestream velocity is lower than rated and vice-versa. In addition, we show that the thrust generated by the turbine remains constant despite significant changes in the freestream velocity. Moreover, the power and thrust generated by such a turbine are observed to be insensitive to yaw, suggesting that this technology can be used to overcome issues arising from misalignment between the turbine and the incoming current. Finally, we use these results to simulate the performance of two turbines in response to low-frequency changes such as those encountered over a tidal period: one equipped with an industry-standard pitch control system, and one with passively pitching blades. The comparison demonstrates that the turbine equipped with passively pitching blades results in the same energy yields as the turbine with active pitch, with the additional benefit of limiting the maximum thrust. Overall, these results suggest that passive pitch control can provide better performances than active pitch control, with an overall simpler and potentially more reliable technology.**

Index Terms—**Tidal turbines, Control systems, Passive pitch.**

I. Introduction

Recent times have seen an unparalleled push in the market towards renewable sources of energy: among these, tidal energy is a promising source as tidal currents are very predictable, not depending on the local weather conditions such as cloud coverage or wind, but instead on periodic tidal effects. Adoption of this source of energy is steadily increasing in the United Kingdom and in Europe: for instance, currently leased tidal sites in Scotland alone could provide up to 1.1 GW of power to the National Grid [3], and the largest individual sites such as the Alderney Race or the Pentlands Firth can potentially provide more than 2 GW individually [4], [5]. However, further expansion of tidal farms is limited by the unsteady flow that characterises these locations, which is turbulent in nature [6], inducing highly unsteady and inhomogeneous loads over the turbine structures. These unsteady loads increase the fatigue loads on turbines [7], and so manufacturers oversize the turbine structures, which in turn drives up costs.

To alleviate these loads, Viola et al. [8] have introduced the concept of passively pitching blades, where the blades of an axial tidal turbine are not mounted rigidly on the turbine structure: instead, an elastic component such as a torsional spring provides a degree of freedom to the blades, which are allowed to pitch around a radial axis. With this arrangement, each blade individually reduces its angle of attack when subject to above-design loads and, conversely, increases its angle of attack when the load reduces, thus opposing changes in the generated loads. Further studies by means of reduced-order codes [1], Computational Fluid Dynamics (CFD) [9], and model-scale experimental testing [2] have shown the potential of this system to limit unsteady loads due to turbulence.

Current industry practice is to use active pitch control. The primary scope of these systems is to control the power transmitted to the generator over the tidal period, so that the power generated by the turbine is always either the maximum that can be harvested given the instantaneous conditions or the maximum the turbine generator can tolerate. Therefore, active pitch is typically used to mitigate relatively low-frequency and large-amplitude changes in free stream velocity, while previous studies on passive pitching focused on relatively high-frequency and low-amplitude changes in the flow velocity experienced by the blade. In contrast, here we show that passive pitch also allows a similar power and thrust control to that achieved with active pitch.

To this end, we present an engineering model that can be used to predict the changes in the performance of a passively pitching blade subject to an arbitrary change in inflow, with the purpose of identifying the best geometry for a pitching turbine blade given the design constraints. Moreover, we show the results of a

This work was supported by the UK Engineering and Physical Sciences Research Council through the grant 'Morphing-Blades: New-Concept Turbine Blades for Unsteady Load Mitigation' [EP/V009443/1]

SG, SO, YL, EMcC, and IMV are with the School of Engineering, University of Edinburgh, Edinburgh EH9 3BF, UK (e-mail for correspondence: I.M.Viola@ed.ac.uk).

AY is with the Department of Mechanical Engineering, University of Bath, Bath, BA2 7AY, UK.

RB and MF are with the Institute for Marine Engineering, National Research Council, Rome 00128, Italy.

Digital Object Identifier:
https://doi.org/10.36688/ewtec-2023-504

novel experimental campaign in which a model-scale tidal turbine is subject to different inflow conditions, in which the freestream speed, the tip-speed ratio, and the yaw angle of the turbine are changed to simulate different conditions in the field, offering comparisons with the engineering model developed. Finally, we build on the experimental and numerical results to predict the performance of a passively pitching turbine over a tidal cycle, and we compare the predicted results to simulations of an industry-standard machine equipped with active pitch control. Results reported here show that passive pitching technology can provide the same performance as actively pitching turbines over a tidal cycle, decreasing the overall system complexity, which is likely to result in higher reliability and lower costs. This, along with the findings from previous literature, show that passive pitch allow mitigation of fast load fluctuations as well as control of the power and thrust over the tidal period, and thus is a promising technology that can increase reliability and reduce the levelised cost of energy.

II. Experimental methodology

A. Facility

The experimental campaign was carried out in the large recirculating water channel at the Institute for Marine Engineering of the Italian National Research Council, in Rome, Italy. This facility is often used for model-scale tests of propellers and ships (see, for instance, [10], [11]), and has a test section with a rectangular cross-section of size 3.6 m $\times$ 2.25 m and a usable length of $10\,\mathrm{m}$; previous studies have found a turbulence intensity of $4\,\%$ and negligible shear [10], [12]. The water temperature is measured by a thermocouple immersed in water; this measurement is then used to estimate the water density ρ and kinematic viscosity ν according to the relations presented by [13] and [14] respectively.

B. Turbine and passive pitching mechanism

The turbine used in this experimental campaign is a speed-controlled, three-bladed turbine with a rotor diameter $D = 1.2\,\mathrm{m}$. The turbine was placed in the test section so that the hub was at a distance from the free surface of $0.8\,\mathrm{m} = 0.67D$, with the turbine tip submerged by $0.2\,\mathrm{m} = 0.17D$; the structure is suspended on rails that sit above the test section. The turbine was tested with freestream speeds U_∞ between $0.4\,\mathrm{m\,s^{-1}}$ and $0.7\,\mathrm{m\,s^{-1}}$; giving a range of diameter-based Reynolds numbers Re of 2.4×10^6 to 4.2×10^6, where

$$Re = \frac{U_\infty D}{\nu}\,. \tag{1}$$

The main components of the turbine are outlined in fig. 1, along with the main reference frame used during this work. This is a cylindrical reference frame rotating with the turbine, having as its axis the turbine rotor axis: distances along this direction are represented by the coordinate X, with its origin on the rotor-swept plane; the radial coordinate is denoted with r and the azimuthal coordinate (out-of-plane in fig. 1) is labelled ψ. As the blades used here are free to pitch, the rotor-swept plane is defined as the plane swept by the pitching axes during the turbine rotation; in this reference frame, the pitching axes are the straight lines at $X = 0, \psi = n\,2\pi/3$, where $n = 0, 1, 2$. The turbine blades (A) are mounted on the pitching systems (B) (described in more detail in fig. 2 and the following paragraphs), which are themselves secured to the common hub (C). The hub is mounted directly on a bespoke load transducer manufactured by Applied Measurements, which has been used to measure the torque and thrust generated by the turbine rotor. The signals from the transducer are then routed through the slip-ring assembly (E), via a cable to a data acquisition board, while the turbine shaft is connected to a DC motor-generator (F).

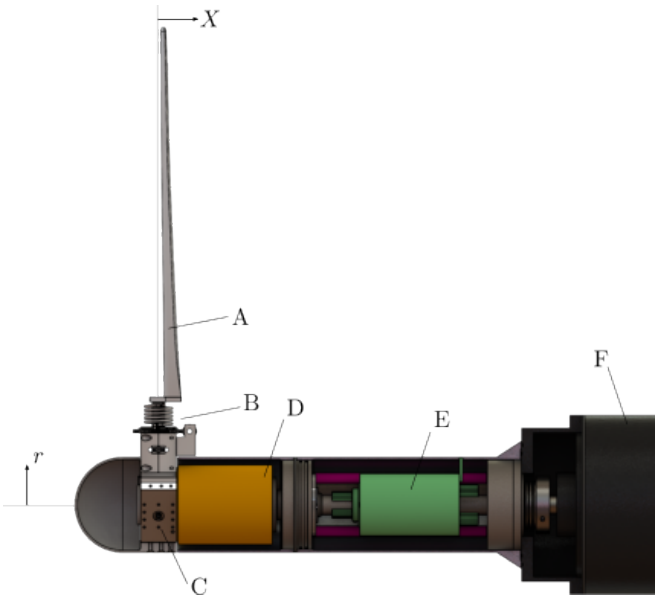

Fig. 1. Sketch of the turbine used during this experimental campaign with annotated components: (A) turbine blade; (B) passive pitching system; (C) turbine hub; (D) load cell and transducer; (E) slip ring assembly; (F) brushless DC generator. Fairings are shown in sectioned view for clarity.

The passive pitching apparatus is shown in fig. 2 in exploded view. The turbine blade (A) is mounted on a spacing arm (B), which separates the blade and the pitching axis (E); by changing the mounting arm it is possible to change the position of the blade with respect to the pitching axis, and thus alter the performance of the system. The rotation of the pitching axis (and therefore of the blade) is constrained by two components: the torsion spring (C) and a retention and limiting screw (I). The torsion spring is manufactured so that its legs extend axially: these engage at the top end with a hole in the mounting arm, and at the bottom end with holes on the top face of a spur gear (D); this gear in turn engages with a worm (K), which locks the rotation of the spur gear. The worm is mounted on the frame (J) by means of a bolt (not pictured). The bolt is turned manually by means of a key: this turns the worm and consequently the spur gear and the bottom leg of the spring, effectively setting the preload of this system. The shaft is constrained by the retention and limiting screw, which is engaged on a threaded hole

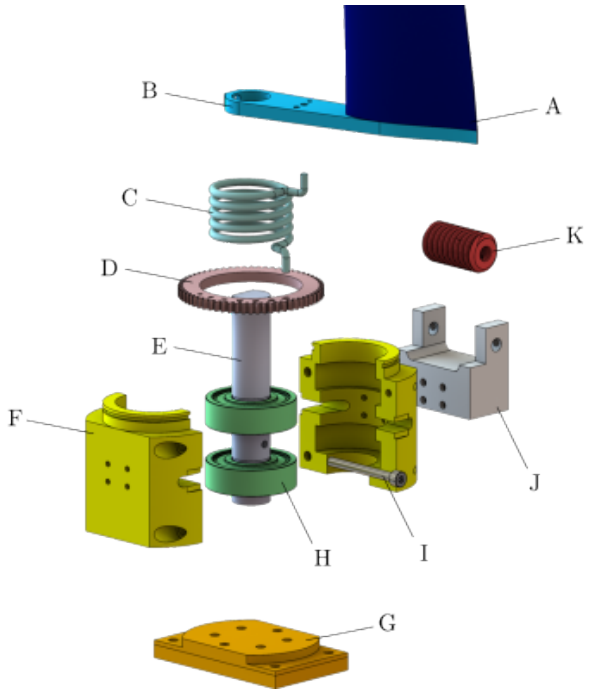

Fig. 2. Exploded view of the passive pitching mechanism, with annotated components: (A) turbine blade; (B) spacing arm; (C) torsion spring; (D) preload spur gear; (E) pitching shaft; (F) mechanism frame; (G) mounting plates; (H) ball bearings; (I) retention and limiting screw; (J) preload worm mounting frame; (K) preload worm.

TABLE I
BLADE TABLE, REPORTING THE RADIAL POSITION OF EACH SECTION r, THE LOCAL CHORD c, TWIST θ, AND THICKNESS t, ALONG WITH THE POSITION OF THE QUARTER-CHORD OF EACH SECTION RELATIVE TO THE PITCHING AXIS x_P AND y_P.

r/D	c/D	θ [°]	t/c	x_P/c	y_P/c
0.115	0.112	17.62	0.24	-1.00	0.11
0.125	0.112	15.66	0.24	-1.00	0.08
0.150	0.111	12.35	0.23	-1.00	0.03
0.175	0.108	10.87	0.23	-1.00	0.01
0.200	0.105	9.96	0.22	-1.00	0
0.250	0.099	8.91	0.20	-1.00	0
0.300	0.093	8.00	0.19	-1.00	0
0.350	0.088	7.03	0.17	-1.00	0
0.400	0.086	6.21	0.16	-1.00	0
0.450	0.083	5.74	0.14	-1.00	0
0.495	0.073	5.50	0.13	-1.00	0

on the shaft: as the shaft rotates, the screw moves in a slot cut in the two frame halves (F), constraining the shaft rotation to a range of 25° in each direction. Alternatively, the screw can be fastened until the screw head engages on a flat surface cut on the frame halves: under this configuration, the shaft is prevented from rotating and the system behaves as a canonical rigid blade.

The turbine blade geometry is given in table I: this reports, for a number of radial stations along the blade at a distance r from the turbine axis, the local chord c, the local twist θ (measured as the angle between the local chord and the rotor-swept plane, positive if the leading edge is upwind), the local thickness t and the position of the section quarter chord relative to the pitching axis of the turbine x_P and y_P. These

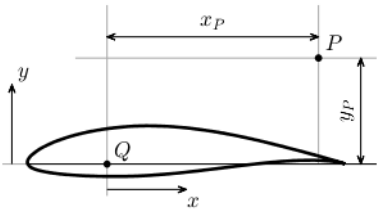

Fig. 3. Definition of the section-based reference frame, along with x_P and y_P for a blade section: Q is the quarter-chord of the particular section and P is the intersection between the pitching axis and the section plane. In this case, both x_P and y_P are positive values.

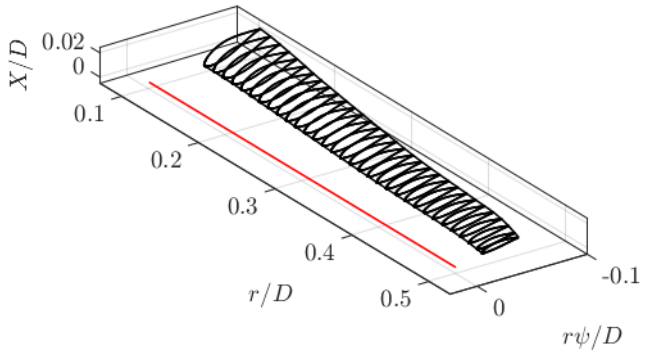

Fig. 4. Three-dimensional representation of the blade sections (*black*) and their position relative to the pitching axis (*red*).

last quantities are measured as the schematic in fig. 3: x_P is the distance along a direction parallel to the section chord between the section quarter-chord Q and the pitching axis P, while y_P is similarly measured in a direction perpendicular to the local chord; x_P is positive if the pitching axis is behind the quarter-chord (going towards the foil trailing edge), and y_P is positive if the pitching axis is above the chord (going towards the suction side of the foil). As x_P is negative for all blade sections, the blade pitches around an axis located ahead of the blade. Note that fig. 3 also defines a reference frame in the section plane, whose coordinates are denoted by lowercase letters: in this, x represents the coordinate along the chordwise direction, positive from the trailing to the leading edge, and y represents the chord-normal coordinate, positive from the pressure to the suction side. This coordinate system has its origin on the quarter-chord of each section, and moves with the section as it pitches. The geometry of the blade is reported in fig. 4, which shows a selection of the blade sections, along with the location of the pitching axis with respect to the blade in solid red; a full 3D model of the blade is available upon request. All sections of the turbine blade are aerofoils belonging to the NACA 63-8XX family, where the last two digits are, in hundredths, the thickness-to-chord ratio t/c.

C. Data acquisition chain

The data acquired in this experimental campaign consists of the thrust T and torque Q generated by the turbine at different values of either freestream speed U_∞ or turbine tip-speed ratio

$$\lambda = \frac{\omega\, r_{\text{tip}}}{U_\infty}\,, \tag{2}$$

where ω is the turbine angular velocity and $r_{\text{tip}} = D/2$. These are acquired by a force and torque transducer (component D in fig. 1) mounted as described above; thus, the measured loads are those generated by all three blades, with no individual information on the loads generated by each single blade. When these loads are presented as functions of the tip-speed ratio, they are reported as the thrust C_T and power coefficient C_P, which are defined as

$$C_T = \frac{T}{\frac{1}{2}\rho U_\infty^2\, \pi r_{\text{tip}}^2}\,, \tag{3}$$

$$C_P = \frac{Q\,\omega}{\frac{1}{2}\rho U_\infty^3\, \pi r_{\text{tip}}^2}\,, \tag{4}$$

having estimated the mechanical power generated by the turbine aszero

$$P = Q\,\omega\,. \tag{5}$$

For each data point, the free stream speed and the turbine angular velocity (and thus the tip-speed ratio) are kept constant.

The angular velocity ω, which is mandated by the DC machine controller, is measured by means of an incremental rotary encoder mounted on the machine shaft. The force and torque transducer is a bespoke load cell manufactured by Applied Measurements Ltd. Calibration of this transducer has been carried out by the manufacturer, and no further efforts to calibrate it have been carried out; the relationship between the load cell current output and the acquired forces is linear. Measurements of the loads are acquired from the load cell by taking the difference in the output of the load cell under load and its mean output under no load, that is a zero reading; such a reading is taken at least once per day with the facility stopped and no flow circulating in the test section. The output of this load cell consists in two $4\,\text{mA}$ to $20\,\text{mA}$ signals that are transferred, via the slip-ring, to a data acquisition board: this is a National Instruments cDAQ system fitted with a NI-9203 board to digitise these analogue signals. Data were acquired at a frequency of $500\,\text{Hz}$ for a duration of $60\,\text{s}$ for the load cell zero readings and $300\,\text{s}$ for the force and torque acquisitions. The acquisition time for each data point was sufficiently large to guarantee convergence of the mean to $\pm 1\%$ of the presented value.

III. Numerical methodology

A. Blade element-momentum theory code

The blade element-momentum theory (BEMT) code that is used in this study is an in-house implementation of the equations of Ning [15], which has been named transTide and previously published in [16]. This code has been further modified since publication by allowing for the definition of different polar curves along the blade span.

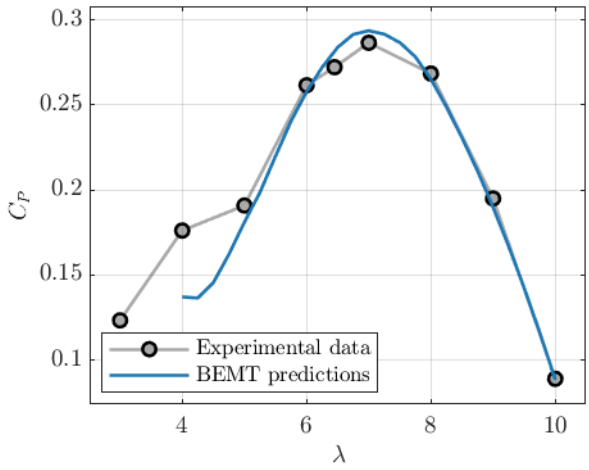

Fig. 5. Comparison between the power estimated by the BEMT code (blue) and the measured data with rigid blades (grey).

The polar curves used in this study have been computed with XFOIL [17]. For each section of the blade, XFOIL is used to compute two polar curves, that is curves that describe the dependency of the lift, drag, and pitching moment coefficient (C_l, C_d, and C_m respectively) as a function of the angle of attack α in the range from $-5°$ to $20°$, with the method of [18] being used to extrapolate outside this range. The first set of polars mimics the behaviour at low-Reynolds by imposing a boundary layer transition at $x_{\text{tr}}/c = 2/3$, while the second set imposes $x_{\text{tr}}/c = 1/4$; the chord-based Reynolds number is computed as

$$Re_c = \frac{U_\infty \sqrt{1 + \left(\frac{\lambda_c r}{r_{\text{tip}}}\right)^2}\, c}{\nu}\,, \tag{6}$$

where $U_\infty = 0.5\,\text{m}\,\text{s}^{-1}$ and λ_c is $\lambda_1 = 4$ for the first set and $\lambda_2 = 8$ for the second set. The generic $C_l(\alpha)$ curve for an aerofoil operating at tip-speed ratio λ is then found as

$$C_l = [1 - w(\lambda)]\; C_l^{(1)} + w(\lambda)\, C_l^{(2)}\,, \tag{7}$$

where $w(\lambda)$ is a weighing function defined as

$$w(\lambda) = \begin{cases} 0 & \lambda < \lambda_1 \\ \frac{1}{2}\left[1 - \cos\left(\pi \frac{\lambda - \lambda_1}{\lambda_2 - \lambda_1}\right)\right] & \lambda_1 < \lambda < \lambda_2 \\ 1 & \lambda_2 < \lambda \end{cases}. \tag{8}$$

The same procedure is used for the drag and moment coefficient.

The inflow simulated is a laminar, non-sheared inflow without surface waves to replicate the experimental conditions in the facility.

Fig. 5 reports the comparison between the power estimated by the BEMT code and the experimentally measured values: it can be seen that good agreement is present between these two sets of data, especially in the case of $\lambda \geq 5$, confirming the validity of the BEMT approach.

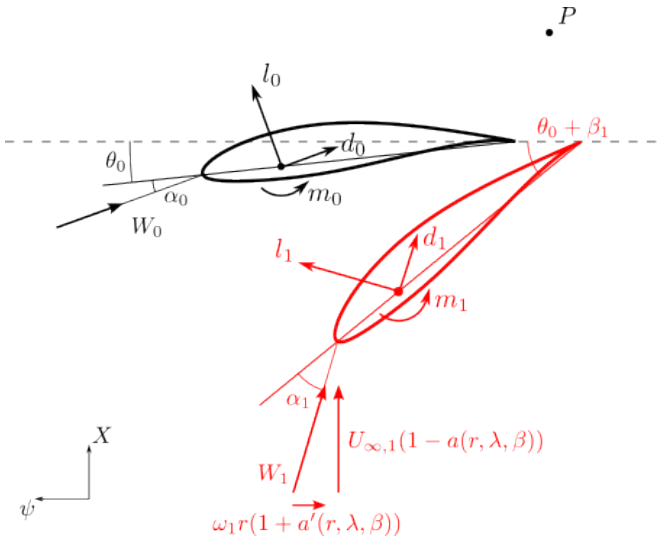

Fig. 6. Position of a section of the pitching blade before (black) and after (red) a change in inflow conditions, along with inflow velocities W, forces per unit span (l, d) and moment around the quarter-chord (m).

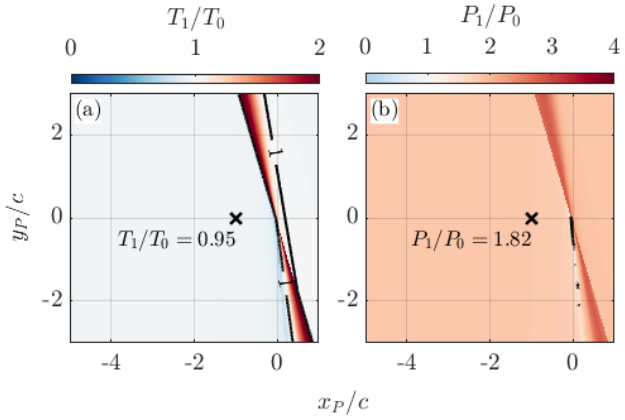

Fig. 7. Ratio of total thrust (a) and power (b) after the change in inflow specified in the text to the values before the change (colour maps), along with value at $x_P/c = -1$, $y_P/c = 0$ and locus of points for which the ratio is unity (black isoline).

B. Mathematical framework for pitching blades

In order to determine the optimal shape of a passively pitching turbine blade, i.e., the location of each section with respect to the pitching axis, one must understand how the choice of pitching axis affects the loads generated by the turbine blade. To do this, we propose the following approach: consider a blade section as pictured in fig. 6, which is subject to an inflow velocity vector $\boldsymbol{W}$ - the resultant of the streamwise (axial) and azimuthal component

$$\boldsymbol{W} = U_\infty \left[1 - a(r, \lambda, \beta)\right] \boldsymbol{e}_X + \omega\, r \left[1 + a'(r, \lambda, \beta)\right] \boldsymbol{e}_\psi \,, \tag{9}$$

where a and a' are the axial and tangential induction factors respectively, $\boldsymbol{e}_X$ and $\boldsymbol{e}_\psi$ are the unit vectors in the axial and azimuthal directions, and β is the pitch angle of the whole blade. Note that, as the blade pitches, the blade induction factors change because the geometry of the blade changes; the dependency of the induction factors on β can be computed as the solution of the BEMT equations by stating that the twist at each section is the sum of the geometrical twist $\theta(r)$ and the pitch β. The moment generated by this section around the pitching axis is

$$m_P(r) = f_x\, y_P - f_y\, x_P + m \,, \tag{10}$$

where, for convenience, we define the terms f_x and f_y as

$$\begin{bmatrix} f_x \\ f_y \end{bmatrix} = \begin{bmatrix} -\sin(\alpha) & \cos(\alpha) \\ \cos(\alpha) & \sin(\alpha) \end{bmatrix} \begin{bmatrix} l \\ d \end{bmatrix} \,, \tag{11}$$

and the forces and moments generated by the section per unit span are defined as

$$l(r) = \frac{1}{2} \rho\, W^2(r, \lambda, \beta)\, c(r)\, C_l(\alpha, r, \lambda) \,, \tag{12}$$

$$d(r) = \frac{1}{2} \rho\, W^2(r, \lambda, \beta)\, c(r)\, C_d(\alpha, r, \lambda) \,, \tag{13}$$

$$m(r) = \frac{1}{2} \rho\, W^2(r, \lambda, \beta)\, c^2(r)\, C_m(\alpha, r, \lambda) \,. \tag{14}$$

The total pitching moment of the blade is

$$M_P = \int_{r_{\text{hub}}}^{r_{\text{tip}}} m_P(r)\, dr \,, \tag{15}$$

where r_{hub} is the station closest to the turbine hub. In the setup presented here, M_P is opposed by the spring moment M_S; in this section, M_S is further assumed constant to simplify the mathematical notation. Denoting with subscript 0 all values before the change in operating conditions and with 1 those after the change, we can find the final pitch angle β_1 by imposing the balance of pitching moments before and after the change:

$$\begin{cases} M_{P,1} = M_S \\ M_{P,0} = M_S \end{cases} \Rightarrow M_{P,1} = M_{P,0} \,, \tag{16}$$

where $M_{P,0}$ is known to have $\beta_0 = 0$ by definition. Note that M_P is a non-trivial function of β, as a change in β changes the induction factors, and therefore both W and α in eqns. (12) to (14), and therefore numerical methods must be used to find this solution. In this work, we simply proceed by exhaustive search: we solve the BEMT equations on a Cartesian space consisting of $r \in [r_{\text{hub}}, r_{\text{tip}}]$, $\lambda \in [4, 10]$, and $\beta \in [-10°, 20°]$; for each point, we calculate $M_{P,1}$ knowing $U_{\infty,1}$ and ω_1 and thus the resulting β_1 as the only value for which $M_{P,1} = M_{P,0}$. Once β_1 is known, one can use eqns. (12) to (14) to estimate the distributions of loads on the blade and their integrals over r to compute the total performance of the turbine.

For this work, we are interested in the particular case for which the turbine undergoes a change in the freestream speed U_∞ during the tidal cycle, while keeping its angular velocity constant. In particular, for this, we impose $U_{\infty,0} = 0.5\,\text{m s}^{-1}$, $U_{\infty,1} = 0.7\,\text{m s}^{-1}$, and $\omega_0 = \omega_1 = 5.375\,\text{rad/s}$. Moreover, we limit our analysis to the distributions for which x_P/c and y_P/c are constant along the blade span. Fig. 7 reports the values of thrust and power generated by the turbine after the change in inflow conditions, both normalised

by the conditions before the gust. It can be seen that there is a large region, upstream of the blade, for which the performance after the change in flow speed is insensitive to the actual position of the blade with respect to the pitching axis; in the figure, we report the values of thrust and power for $x_P/c = -1$ and $y_P/c = 0$ as reference. There is also a narrow region closer to the blade where the turbine performance after the inflow change is highly sensitive to the actual values of x_P and y_P. In principle, there exists a locus of points for which the thrust does not vary with this particular inflow change; however, any deviation from the idealised conditions, due for instance to manufacturing defects, errors in the BEMT solution, or inflow changes different from those assumed here, might give rise to very different behaviour in the field, and thus solutions close to the high-sensitivity region should be discarded. For this reason, it was decided to manufacture a blade that has a constant $x_P/c = -1$ and $y_P/c = 0$, as reported in table I. For ease of manufacture, it was also decided to shift the profiles close to the root in the y-direction, so that the blade geometry would not be excessively swept in the flapwise direction.

IV. Results

Two runs were carried out to measure the thrust and the power generated by the tidal turbine under different conditions. First, the freestream speed was changed in the range of $U_\infty = 0.4\,\mathrm{m\,s^{-1}}$ to $0.7\,\mathrm{m\,s^{-1}}$ with the angular velocity held constant at $\omega = 5.37\,\mathrm{rad\,s^{-1}}$, such that the tip-speed ratio changed accordingly. The second run spanned the tip-speed ratio in the range of $\lambda = 3$ to 10 by altering the angular velocity while holding $U_\infty = 0.5\,\mathrm{m\,s^{-1}}$ constant. A point at $\lambda = 6.45$, $U_\infty = 0.5\,\mathrm{m\,s^{-1}}$ is shared between these two runs; the values of thrust and power generated by the turbine equipped with pitching blades under no yaw at this operating point have been taken as reference and are labelled T_{ref} and P_{ref} respectively in this section, while we define $U_{\mathrm{ref}} = 0.5\,\mathrm{m\,s^{-1}}$. These runs were repeated for four configurations, where the blades were either allowed to pitch or rigidly secured to the turbine chassis, and where the turbine axis was either aligned with the direction of the freestream or a yaw angle $\gamma = 15^\circ$ was introduced. For the runs where the blades were allowed to pitch, the springs were preloaded by 447.5°, and the maximum pitch angle was limited to $\pm 25^\circ$ by the retention slot (see fig. 2). Under these conditions, it can be assumed the spring moment is essentially constant and the results are independent of the spring used.

A. Turbine performance in absence of yaw

Fig. 8 reports the measured thrust and power generated by the turbine with either rigid or passively pitching blades in either a regime of constant angular velocity (above) or constant freestream speed (below). One can readily observe that at U_{ref} the thrust and power of the rigid and passively pitching turbine do not match: this is likely due to an erroneous estimation of the preload of the spring used to constrain the motion of the blades, which has eventually resulted in a non-zero pitch of the blades. This might be due to uncertainty in the spring elastic constant, which has only been estimated with an engineering formula. Nonetheless, the observations that can be gathered from these results are not affected, as the spring preload β_{pre}, and therefore the mean spring moment M_S, has not been changed during the course of the tests.

It can be seen that the thrust generated by the turbine with pitching blades is markedly steady over a large range of operating conditions: for the run at constant angular velocity, the thrust is always lower than that of the reference point, with a minimum at the smallest value of U_∞ tested of $0.85T_{\mathrm{ref}}$ and an approximately constant value for $U_\infty > U_{\mathrm{ref}}$. For the operating conditions with variable λ, it can also be seen that the thrust coefficient of the turbine with pitching blades is bounded in a narrow interval between approximately 0.5 and 0.65. Both these plots compare positively to the trends seen for the same operating conditions with the rigidly mounted blades: the range of both thrust and C_T values attained have smaller minima and larger maxima. A turbine equipped with passively pitching blades is therefore naturally capping the thrust generated to that of the design operating point, here represented by T_{ref}.

Turning now to the power data, it is evident that the power generated by the turbine with pitching blades still follows an increasing trend with freestream speed U_∞; however, the slope of this trend is smaller than that of its rigid counterpart, and the generated power is therefore less sensitive to the inflow conditions for a turbine equipped with passively pitching blades, as predicted by the maps in 7(b).

As an additional remark, one can observe that C_P tends to negative values as the tip-speed ratio decreases for the case of pitching blades. As the tip-speed ratio decreases, the total velocity seen by the blade sections decreases and with it the moment around the pitching axis; the constant balancing moment of the spring pitches the blade to negative values of β, thus increasing the angle of attack over the blade further. In the limit, at $\omega = 0$ and therefore $\lambda = 0$, the blade pitches to the minimum angle allowed by the retention mechanism, which is -25° for this implementation; under these conditions, the flow around the turbine blade is stalled and no usable torque is generated. This result suggests that particular care must be given to the design of the pitching mechanism to ensure that, at low speeds (and to the limit at $\omega = 0$), the turbine generates positive power (and therefore torque) and can self-start.

The thrust and power predicted by the BEMT code are included in fig. 8 as blue lines. Considering first the thrust and power measurements at varying U_∞(upper plots), the predictions of the reduced-order code match the experimental results well for $U_\infty/U_{\mathrm{ref}} \geq 1$. For velocities lower than U_{ref}, instead, the predictions are less accurate but still valid: for example, the low-order code approach cannot accurately capture the departure from the linear trend of $T(U_\infty)$ at low velocities. This change in behaviour is likely due to the friction in-

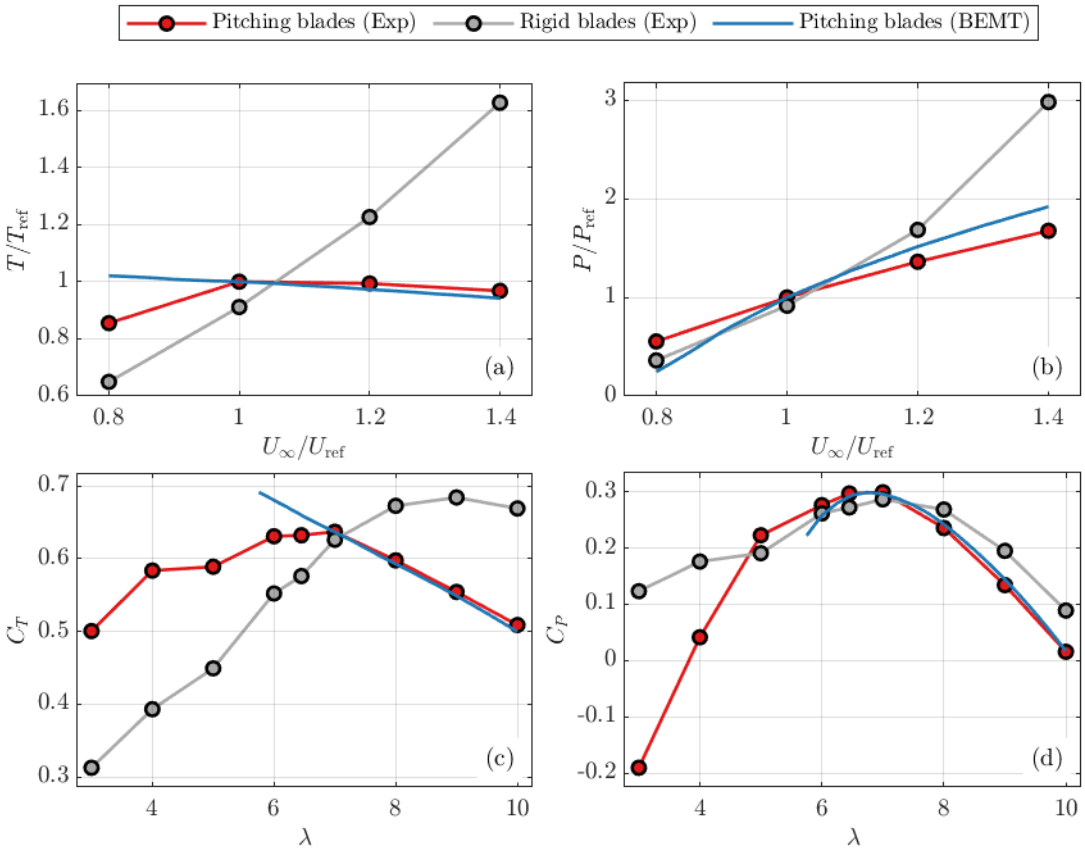

Fig. 8. Above: thrust (a) and power (b) generated by the turbine under constant angular velocity and variable freestream speed. Below: thrust (c) and power (d) generated by the turbine under constant freestream speed and changing tip-speed ratio. Data for the runs at zero yaw: turbine equipped with rigid blades (grey), with pitching blades (red), and estimates of the performance with pitching blades by the BEMT code of sec. III-B.

troduced by the bearings securing the pitching axis in place: as previously observed in [2], the performance of the passively pitching blade is strongly affected by friction. The hydrodynamic moment generated by the blades around the pitching axis decreases quadratically with U_∞, while the friction around the shaft is approximately constant: as such, the predictions of the low-order code, which does not account for friction, are less accurate for low values of U_∞. Similar observations can be made for the test case of constant U_∞ and varying λ, for which the BEMT code provides accurate predictions of the turbine behaviour at high values of λ, which confirms the validity of this approach for design purposes.

B. Turbine performance in the presence of yaw

Fig. 9 reports the thrust and power generated by the turbine under the same set of inflow conditions as in the previous section, but this time with and without yawed inflow ($\gamma = 15°$). T_{ref} and P_{ref} are the same values as used in fig. 8. It can be seen that both the thrust and the power generated by the turbine equipped with pitching blades are only minimally affected by the large yaw angle, as all performance figures match well. Some minor differences between the two pitching test cases however are present: for instance, it can be seen that the thrust generated by the turbine slightly increases with increasing U_∞ for the case where yaw is present, while this is not observed for the $\gamma = 0$ test case; however, this increase is minor, amounting only to $3\,\%$ of T_{ref} at $U_\infty/U_{\text{ref}} = 1.4$. Likewise, the power of the pitching blade under yaw appears to be larger than that at $\gamma = 0$ for high U_∞ and lower at low freestream speed, being closer to those obtained with the rigid blade; however, this is a small difference between the two pitching blade datasets, and is within the experimental uncertainty.

In comparison, the thrust and power generated by the turbine equipped with rigid blades have decreased by a constant factor of $\cos^2(15°)$ and $\cos^3(15°)$ respectively. Note that, for the yawed test cases, no comparison with BEMT predictions is offered as the theoretical background presented in sec. III-B does not account for the presence of yaw.

C. Predicted performance over a tidal period

Having observed the performance of the passive pitch system, and in particular the trends of power and thrust as functions of the freestream speed U_∞, one can estimate the loads and performance generated by a turbine equipped with passively pitching blades in a realistic inflow. To gauge how this passive control system compares to current state-of-the-art in terms of speed- and pitch-controlled turbines, we use the BEMT data previously shown to simulate two synthetic turbines harvesting power from an idealised, sinusoidal

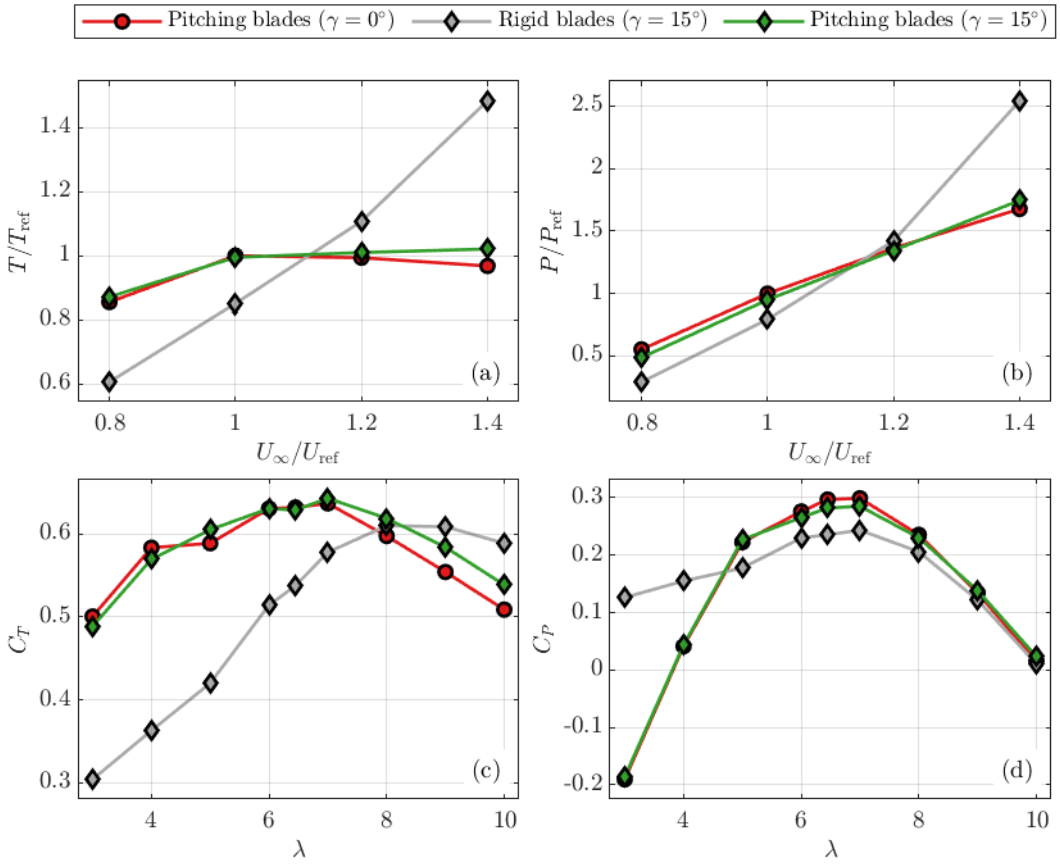

Fig. 9. Above: thrust (a) and power (b) generated by the turbine under constant angular velocity and variable freestream speed. Below: thrust (c) and power (d) generated by the turbine under constant freestream speed and changing tip-speed ratio. Data for: turbine equipped with pitching blades at $\gamma = 0°$ (red), with rigid blades at $\gamma = 15°$ (grey), and with pitching blades at $\gamma = 15°$ (green).

flow representative of the flow seen by a tidal turbine during a tidal cycle. The sinusoidal flow here used follows the time history

$$\frac{U_\infty(t)}{U_{\text{ref}}} = \frac{U_{\text{rated}}}{U_\infty} - 0.2\cos\left(2\pi\frac{t}{\tau}\right) \quad t \in [0;\tau]\,, \qquad (17)$$

where τ is the tidal period, U_{rated} is here chosen to be $1.2\,U_{\text{ref}}$ and the amplitude is chosen so that $U_\infty/U_{\text{ref}} \in [1;1.4]$ as experimental data from the tidal turbine equipped with pitching blades is available, where $U_{\text{ref}} = 0.5\,\text{m}\,\text{s}^{-1}$ for consistency with previously presented results.

The state-of-the-art is represented by a speed- and pitch-controlled turbine, whose controller aims to keep the harvested power below a maximum value P_{rated}, which is itself computed as the maximum power the turbine can harvest when $U_\infty = U_{\text{rated}}$. For freestream speeds below U_{rated}, the controller sets both the tip-speed ratio λ and the blade pitch β to maximise the generated power; for higher speeds, the controller keeps $P = P_{\text{rated}}$ by mandating a constant angular velocity ω_{rated} and increasing the blade pitch. The tip-speed ratio λ_{rated} is the value of λ at which the turbine operates for $U_\infty \to U_{\text{rated}}$.

The current passively pitching turbine is modelled as a speed-controlled turbine in which the pitch angle β is not mandated by the controller, but inferred for each operating condition from eqn. (16). As with the state-of-the-art, the controller maximises the power generated by the turbine for $U_\infty < U_{\text{rated}}$, and keeps $P = P_{\text{rated}}$ for $U_\infty > U_{\text{rated}}$ by increasing the pitch angle; as direct control of the pitch is unavailable, the increase in β is obtained by increasing the turbine angular velocity, and therefore by increasing λ. The spring preload is set so the blade has a pitch angle β of 0° when $U_\infty = U_{\text{rated}}$ and $\lambda = \lambda_{\text{rated}}$.

The time-histories of the angular velocity and the generated loads are reported in fig. 10, where the loads generated by the actively controlled turbine are reported in red and those of the currently tested turbine are reported in blue. It can be immediately seen that the turbine equipped with passively pitching blades is able, by means of only controlling the turbine angular velocity, to track the power generated by the actively controlled turbine, as shown in fig. 10(c): in fact, the two time-histories of generated power match well over the whole tidal period, except when $U \approx U_{\text{ref}}$, where a slight loss in power is observed. Conversely, the thrust time-histories are visibly different, as seen in fig. 10(d): the passively pitching turbine manages to generate both a lower maximum value of thrust and a lower variation in thrust over the whole tidal period. This reduction in thrust comes at a cost of a more complicated angular velocity controller: as it can be seen in fig. 10(b), the rotor speed is not constant for $U_\infty > U_{\text{rated}}$: as U_∞increases, the blades must increase their pitch to reduce their angle of attack and ultimately keep the power constant, which is achieved by

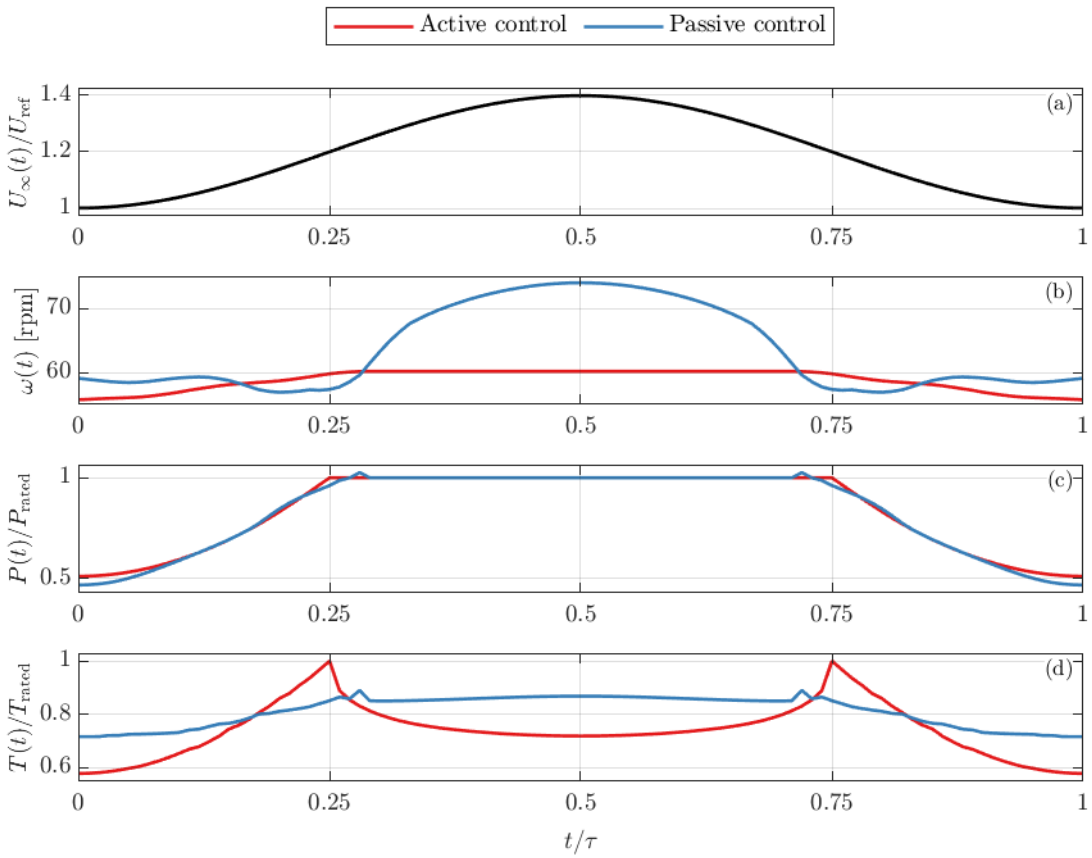

Fig. 10. Performance of an actively controlled tidal turbine (red) and a speed-controlled passive pitch turbine (blue) over a simulated tidal cycle. From top to bottom: freestream speed (a), angular velocity (b), power (c) and thrust (d) generated.

increasing ω.

V. Conclusions

In this paper, we have investigated the effects of a steady change in inflow and operating conditions on the time-averaged performance of a model scale tidal turbine equipped with passively pitching blades. The results here presented include the outputs of a low-order code based on the well-established blade element-momentum theory as well as the measurements of an experimental campaign carried out in a recirculating water channel.

The reduced-order approach, based on the BEMT and therefore computationally inexpensive, has been used to investigate the optimal geometry of a tidal turbine blade that could limit the changes in the thrust transferred to the turbine structure in the presence of changes in freestream speed. This framework has been used to show that the performance of a turbine after a change in freestream speed is relatively insensitive to the location of the blade with respect to the pitching axis, and therefore to the geometry of the blade. For a blade that pitches about an axis located ahead of its leading edge, the reduced order code predicts that a change in freestream speed does not appreciably change the thrust generated by the blade, while reducing the power increase. The performance of the blade is most sensitive to the position of its sections relative to the pitching axis in a narrow region located broadly above and below the foils; due to the high sensitivity of both the generated thrust and power, these locations are not recommended for a pitching axis.

The turbine has been tested in a recirculating channel, where the freestream speed, the turbine angular velocity and the turbine yaw were changed. It was observed that the thrust generated by a turbine equipped with passively pitching blades is indeed insensitive to changes in the freestream speed, as an increase of $40\,\%$ in the current speed induces a reduction in the generated thrust of $3\,\%$. The effect of U_∞ changes on the power generated by the turbine is more pronounced, although the power curve is seen to be less sensitive to variations of freestream speed than that of a turbine equipped with rigid blades. Similarly, by analysis of the power and thrust curves as a function of the tip-speed ratio, it was seen that a turbine equipped with such blades is not necessarily self-starting, as the blade moves to large negative values of pitch under no load, and the flow around the blade is stalled at start-up; an observation on how to correctly estimate the range of allowed pitch angles that allow for the turbine to self-start has also been presented here. The predictions of the reduced-order model are seen to match well with the experimental results.

The performance of the turbine has also been tested in the presence of yaw, which was set to 15° for this study. It has been shown that, without changing the spring preload and therefore the settings of the pitching apparatus, the performance of the turbine equipped with pitching blades under yaw matches

particularly well the performance of the same turbine under no yaw: this shows that a turbine equipped with this passive system is insensitive to misalignment between the turbine axis and the freestream.

Finally and most importantly, a simulation of the performance of an ideal passively pitching, actively speed-controlled turbine over a tidal cycle shows that this technology, if deployed in the field, can generate the same power over a tidal cycle (and therefore, a similar annual energy production) to the current industry-standard speed- and pitch- controlled turbine. At the same time, this technology provides an improvement over the state-of-the-art by passively regulating and limiting the thrust generated.

REFERENCES

[1] G. Pisetta, R. Le Mestre, and I. M. Viola, "Morphing blades for tidal turbines: A theoretical study," *Renewable Energy*, vol. 183, pp. 802–819, Jan. 2022.

[2] S. Gambuzza, G. Pisetta, T. Davey, J. Steynor, and I. M. Viola, "Model-scale experiments of passive pitch control for tidal turbines," *Renewable Energy*, vol. 205, pp. 10–29, Mar. 2023.

[3] S. P. Neill, A. Vögler, A. J. Goward-Brown, S. Baston, M. J. Lewis, P. A. Gillibrand, S. Waldman, and D. K. Woolf, "The wave and tidal resource of Scotland," *Renewable Energy*, vol. 114, pp. 3–17, Dec. 2017.

[4] S. Draper, T. A. Adcock, A. G. Borthwick, and G. T. Houlsby, "Estimate of the tidal stream power resource of the Pentland Firth," *Renewable Energy*, vol. 63, pp. 650–657, Mar. 2014.

[5] D. Coles, L. Blunden, and A. Bahaj, "Assessment of the energy extraction potential at tidal sites around the Channel Islands," *Energy*, vol. 124, pp. 171–186, Apr. 2017.

[6] G. T. Scarlett, B. Sellar, T. van den Bremer, and I. M. Viola, "Unsteady hydrodynamics of a full-scale tidal turbine operating in large wave conditions," *Renewable Energy*, vol. 143, pp. 199–213, Dec. 2019.

[7] L. Chen and W.-H. Lam, "A review of survivability and remedial actions of tidal current turbines," *Renewable and Sustainable Energy Reviews*, vol. 43, pp. 891–900, Mar. 2015.

[8] I. M. Viola, G. Pisetta, W. Dai, A. Arredondo-Galeana, A. M. Young, and A. S. M. Smyth, "Morphing blades: Theory and proof of principles," in *Proceedings of the European Wave and Tidal Energy Conference*, Plymouth, United Kingdom, 2021, p. 11.

[9] W. Dai, R. Broglia, and I. M. Viola, "Mitigation of rotor thrust fluctuations through passive pitch," *Journal of Fluids and Structures*, vol. 112, p. 103599, Jul. 2022.

[10] A. Pecoraro, F. Di Felice, M. Felli, F. Salvatore, and M. Viviani, "An improved wake description by higher order velocity statistical moments for single screw vessel," *Ocean Engineering*, vol. 108, pp. 181–190, Nov. 2015.

[11] L. Wang, J. E. Martin, M. Felli, and P. M. Carrica, "Experiments and CFD for the propeller wake of a generic submarine operating near the surface," *Ocean Engineering*, vol. 206, p. 107304, Jun. 2020.

[12] G. Calcagno, F. Di Felice, M. Felli, and F. Pereira, "A Stereo-PIV Investigation of a Propeller's Wake behind a Ship Model in a Large Free-surface Tunnel," *Marine Technology Society Journal*, vol. 39, no. 2, pp. 94–102, Jun. 2005.

[13] M. Tanaka, G. Girard, R. Davis, A. Peuto, and N. Bignell, "Recommended table for the density of water between 0 C and 40 C based on recent experimental reports," *Metrologia*, vol. 38, no. 4, pp. 301–309, Aug. 2001.

[14] L. Korson, W. Drost-Hansen, and F. J. Millero, "Viscosity of water at various temperatures," *J. Phys. Chem.*, vol. 73, no. 1, pp. 34–39, Jan. 1969.

[15] S. A. Ning, "A simple solution method for the blade element momentum equations with guaranteed convergence," *Wind Energy*, vol. 17, no. 9, pp. 1327–1345, 2014.

[16] G. T. Scarlett and I. M. Viola, "Unsteady hydrodynamics of tidal turbine blades," *Renewable Energy*, vol. 146, pp. 843–855, Feb. 2020.

[17] M. Drela, "XFOIL: An Analysis and Design System for Low Reynolds Number Airfoils," in *Low Reynolds Number Aerodynamics*. Springer, Berlin, Heidelberg, 1989, pp. 1–12.

[18] L. A. Viterna and D. C. Janetzke, "Theoretical and experimental power from large horizontal-axis wind turbines," National Aeronautics and Space Administration, Cleveland, OH (USA). Lewis Research Center, Tech. Rep. DOE/NASA/20320-41; NASA-TM-82944, Sep. 1982.